# Multiscale Simulations of Carbon Nanotube Nucleation and Growth: Electronic Structure Calculations

J. C. Wells,[a] D. W. Noid,[a] B. G. Sumpter,[a] R. F. Wood,[b] and Q. Zhang[c]

[a] *Computer Sciences and Mathematics Division, Oak Ridge National Laboratory, Oak Ridge, Tennessee, USA*
[b] *Condensed Matter Sciences Division, Oak Ridge National Laboratory, Oak Ridge, Tennessee, USA*
[c] *Department of Physics, University of Texas, Arlington, Texas, USA*

Several first-principles surface and bulk electronic structure calculations relating to the nucleation and growth of single-wall carbon nanotubes are described. Density-functional theory in various forms is used throughout. In the surface-related calculations, a 38-atom Ni cluster and several low-index Ni surfaces are investigated using pseudopotentials and plane-wave expansions. The energetic ordering of the sites for C atom adsorption is found to be the same, with the Ni(100) facet favored. The bulk diffusion coefficient of C in Ni as a function of cluster size and temperature is calculated from various molecular dynamics approaches. In another group of bulk-related calculations, Gaussian orbital basis sets are used to study a cluster or "flake" containing 14 C atoms. The flake is a segment of three hexagons from an "unrolled" carbon nanotube, with an armchair termination. The binding energies of C, Ni, Co, Fe, Cu, and Au atoms to it were calculated in an effort to gain insight into the mechanism for the high catalytic activity of Ni, Co, and Fe and the lack of it in Cu and Au. The binding energies of Cu and Au are about 1 eV less than those of the three catalytic elements. Similar methods are used to study the initial stages of nanotube growth within the context of classical nucleation theory. Finally, issues relating to the establishment of a fundamental catalytic mechanism are addressed.

**Keywords:** Carbon Nanotubes, Catalysis Electronic Structure, Simulations, Growth.

RESEARCH ARTICLE

## 1. INTRODUCTION

The importance of nanoscience to advanced materials development and the potential opportunities and benefits to be derived from it have been repeatedly emphasized during the last decade and need not be discussed here. Within the nanoscience area, carbon nanotube (CNT) research is arguably the most likely to yield dramatic near-term results if certain issues can be resolved. Paramount among these issues is the role of the metal catalyst, which is still unclear even for the simplest growth technique. In fact, the wide variety of experimental conditions under which nanotubes grow suggests that there may be more than one set of physical and chemical processes by which the catalyst carries out its function, even if the fundamental catalytic step is the same. Many groups using both phenomenological, continuum models[1–6] and first-principles calculations of various types,[7–11] including molecular dynamics (MD), have explored nanotube nucleation and growth. However, the role of the catalyst has been difficult to resolve because of the inherent limitations of the techniques that must necessarily be used. The continuum models do not have the atomic-scale spatial resolution that is needed, satisfactory metal-carbon potentials for classical MD simulations are not yet available, and quantum mechanical MD simulations are still too computer-intensive to allow identification of an elementary dynamical process that might be common to the different growth techniques (e.g., laser ablation, arc fusion, and chemical vapor deposition).

We have recently begun a multiscale simulation research effort to understand the fundamental aspects of the nucleation and growth of CNTs. Our objectives are to develop and apply a suite of advanced computational techniques and computer programs to carry out the simulations. The techniques span multiple time and space domains and use continuum heat and mass transport, first-principles electronic structure, MD, and molecular mechanics calculations. At this workshop, we report on our initial work in both the continuum (mesoscale) and atomistic simulations. Pannala and Wood cover the continuum work in another article in this issue. Here, several different types of first-principles surface and bulk electronic structure calculations are described. We emphasize that we are still at the early stages of this work and the calculations are of a

*Author to whom correspondence should be addressed.

 © 2004 by American Scientific Publishers 1533-4880/2004/04/414/009/$17.00+.25 doi:10.1166/jnn.2004.063

somewhat exploratory nature and also cover a number of different topics that may not seem related at first sight.

The plan of the article is as follows. In the surface-related work of Section 2, a 38-atom Ni cluster and several low-index Ni surfaces were studied with computational methods based on density-functional theory (DFT) using a plane-wave formalism with ultrasoft pseudopotentials. The binding energies of a C atom on various Ni surfaces and the corresponding facets on the Ni cluster were obtained. The work related to bulk processes is described in Sections 3 to 5 Although the calculations are generally based on DFT, we used Gaussian orbital basis sets rather than plane-wave expansions. In Section 3, MD calculations of the bulk diffusion coefficient of C in Ni clusters are presented. As described in Section 4, the binding energies of C, Ni, Co, Fe, Cu, and Au atoms to this flake were calculated in an effort to gain insight into the mechanism for the high catalytic activity of Ni, Co, and Fe and the lack of it in Cu and Au. In Section 5, first-principles calculations that obtain certain quantities appearing in the classical nucleation theory of nanotube growth are described and compared with experimental continuum results. In a suggested nucleation scenario, the role of the transition metal ions is to complete the dangling bonds of the flake and so counteract the strain energy introduced by deforming the flake into the nanotube caps. The calculations indicate that the binding energies of Cu and Au to the C flake are about 1 eV less than those of the three catalytic elements, with the unfilled d shells clearly playing a role. Quantities related to the so-called "scooter" mechanism of nanotube growth are discussed in Section 6. The article ends with a short section summarizing the main results and pointing out future directions.

## 2. ADSORPTION ENERGETICS ON SURFACES

An important common feature in the synthesis of single-walled carbon nanotubes (SWNTs) is that small clusters of certain transition metals (TMs) (e.g., Fe, Co, and Ni) and rare earth metals (Y and La) or their mixtures are used and found to be essential in a high-yield SWNT formation. The morphologies of grown SWNTs are directly related to the particle size. Despite intensive experimental and theoretical studies in the field, the fundamentals of SWNT catalytic growth are still unclear. Questions to be answered include why clusters are effective catalysts rather than extended surfaces. One obvious difference is that a cluster has a variety of facets. The facets may play complementary roles in the catalysis process: one could control feedstock decomposition, whereas others may serve to promote nucleation. To understand these fundamentals, it is worthwhile to determine which facet is the preferred adsorption site for a carbon atom on TM clusters. Such information is difficult to obtain from experiments but is readily available from theoretical analysis. In addition to their interest for SWNT nucleation, studies of TM clusters are of broad scientific interest due to their intrinsic role in heterogeneous catalysis and nanoscale magnetism.

Here we consider Ni and compute adsorption energies (i.e., bonding energies) of C nucleation on Ni surfaces by first-principles methods. We shall focus on the adsorption of 1 C atom on a 38-atom Ni cluster and several low-index Ni surfaces. Information on adsorption energies on TM surfaces serves as a probe of the electronic structure of the TM system and an excellent opportunity for comparison between experiment and theory. The Vienna *ab initio* simulation package, used in the calculations reported in this section, uses DFT under the generalized gradient approximation (GGA) for the exchange-correlation functional using the plane-wave formalism with Vanderbilt ultrasoft pseudopotentials for both Ni and C.[12–14] A kinetic-energy cutoff of 21 Ry is used for the wave functions. For the GGA functional, we used the PW91[15] scheme, which gives satisfactory results in many studies of strong adsorptions on metal surfaces,[16] and we neglected, for the present purposes, the spin degree of freedom, because we are interested here in the general trend of binding energies.[17]

As a test of the accuracy of our approach, $Ni_2$ and $C_2$ have been computed. Our calculated bond lengths (2.05 and 1.26 Å for $Ni_2$ and $C_2$, respectively) are in reasonably good agreement with experimental results (2.155 and 1.253 Å[18]). Our results for the binding energies are 2.8 and 6.6 eV for $Ni_2$ and $C_2$, in comparison to experimental values of 2.07 and 6.2 eV, respectively.[18] Such overprediction of binding energies by DFT is not atypical,[19,20] but more accurate values for TM atomic dimers have been reported.[21] These were obtained by incorporating the effects of nonlinear core-correction in the description of the atoms.[22]

The $Ni_{38}$ cluster geometry was completely relaxed, beginning with an initial geometry with truncated octahedral symmetry. The local optimization procedure maintained this high symmetry without the imposition of constraints. Although the size of the cluster is relatively small, it preserves many crystalline features with three unique, stable adsorption sites. One is the hollow site on the (100) facet. The remaining two are face-centered cubic (fcc) and hexagonal close-packed (hcp) sites on the (111) facet (Fig. 1). The binding energies of a C atom on these three facets on the Ni cluster and on corresponding low-index Ni surfaces are presented in Table I. The magnitude and ordering of the absorption energy with respect to the adsorption site are essentially the same for the cluster and the surface. Typically, nanoclusters are more reactive than surfaces because of reactive edges with morphologies different from those of surfaces. Given the apparently large differences of the two types of substrates (e.g., surface curvature and presence of defect sites), this result is notable and supports the concept of locality of bonding of C atoms to TM substrates.

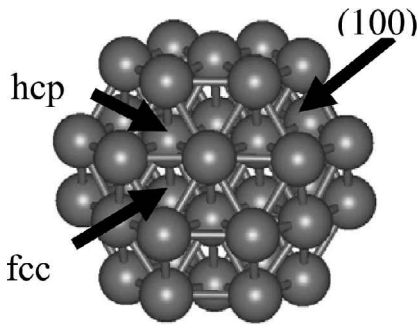


**Fig. 1.** The high-symmetric $Ni_{38}$ cluster has an fcc structure. The three stable adsorption sites are indicated.

The similarity of C binding energies between $Ni_{38}$ and Ni surfaces is qualitatively consistent with available experimental results,[17, 23] but, as anticipated, our DFT calculations overpredict binding energies relative to experimental values. The binding of C to Ni (100) surfaces has been measured and a value of 7.35 eV was found.[24] Recently, the binding of C to $Ni_n$ cluster cations has been measured for $2 \leq n \leq 16$[25] using guided ion beam techniques similar to those used for C bonding to $Fe_n$ cluster cations.[26] (One expects the C-$Ni_n$ bond energies between neutral clusters and cluster cations to be very much the same.) As discussed in Ref. 26 for $Fe^+_n$, the most striking observation in the binding of C to $Ni^+_n$ is that the values for $n \geq 5$ are large and do not vary appreciably (e.g., for $5 \leq n \leq 16$, the average measured binding energy is approximately 6.5 eV).[25] The binding energy as a function of cluster size varies strongly for $n < 5$, and then saturates for $n \geq 5$ to values very close to those for C binding to bulk Ni surfaces. This behavior may be understood in terms of simple bond ordering and atom coordination arguments.[24, 26]

## 3. BULK DIFFUSION OF C IN Ni CLUSTERS

Classical and quantum MD were used to determine the diffusion coefficients of C in Ni clusters as a function of cluster size and temperature. Clusters of 38 to 2000 Ni atoms were generated by optimizing the geometry governed by a semiempirical potential energy surface obtained from a combination of quantum chemistry calculations and experimental data. The simplest form of the potential used only two-body functions for Ni–Ni, Ni–C, and C–C interactions. The functional form was

$$V(r) = D\{1\text{-}\exp[-\alpha(r - r_o)]\}^2 \quad (1)$$

where $D$(Ni–Ni) = 2.08 eV, $D$(Ni–C) = 4.13 eV, $D$(C–C) = 6.21 eV, $r_o$(Ni–Ni) = 2.20 Å, $r_o$(Ni–C) = 1.67 Å, $r_o$(C–C) = 1.24 Å, α(Ni–Ni) = 1.2 $Å^{-1}$, α(Ni–C) = 1.7 $Å^{-1}$, and α(C–C) = 2.2 $Å^{-1}$. These parameters were derived from *ab initio* quantum simulations[27] using DFT (B3LYP 6-311G**) and combined with available experimental data.[28] The numerical techniques used the local spin density approximation and Gaussian orbitals as implemented in the NWChem software collection.[27] Although this potential energy surface is clearly an oversimplification of the actual multibody forces involved, it provides a reasonable approximation of the dominant forces that govern molecular diffusion. Other forms of the potential energy surface that were considered included the use of many-body functions of the form:

$$V(r) = K\,(r - r_o)^2,\ V(\theta) = K_\theta\,(\cos\theta - \cos\theta_o)^2,\ V(\tau) = K_\tau\,[1 - \cos(n\tau)] \quad (2)$$

where $\theta$ is the bending angle between a three-atom sequence and $\tau$ is the dihedral angle between a four-atom sequence. Nonbonded interactions were modeled by a Lennard-Jones 6-12 potential plus a Coulomb contribution:

$$V(r) = 4\sigma\,[\sigma^{12}/r^{12} - \sigma/r^6] + q_1 q_2/\varepsilon_o r \quad (3)$$

Here, $q_1$ and $q_2$ are effective charges and $\varepsilon_o$ is the dielectric constant.

The parameters for the potential functions were taken as defined by the Dreiding-type potential.[29] The accuracy of the Dreiding II force field has been thoroughly tested by comparison with 76 accurately determined crystal structures of organic compounds involving H, C, O, F, P, S, Cl, and Br; rotational barriers of a number of molecules; and relative conformational energies and barriers of several others. This potential is a reasonable starting point for examining the effects of multibody interactions on the diffusion of C in Ni. For all of the classical potential energy surfaces, Hamilton's equations of motion were solved using symplectic integrators (with 1 fs time steps), which ensure robust integration for nearly any time scale.

We considered various cluster sizes, $Ni_n$, with $n$ within the range of several hundred atoms. As an example, the results of the diffusion studies for $Ni_{257}$ are summarized in Figure 2. Reasonably good accord for large nickel clusters was found with experimental bulk diffusion data for metallic carbide systems at room temperature. Somewhat surprising is the fact that the simplest potential energy surface (two-body interactions only) was quantitatively able to predict these data. Similar observations have been reported recently by Lee et al.,[30] for the melting behavior of metallic clusters. The dependence of the diffusion coefficient on temperature shows the typical Arrhenius law behavior for higher temper-

**Table I.** Adsorption energies (in eV) and the coordination number of the Ni atoms at a unique adsorption site of a carbon atom on the $Ni_{38}$ cluster (see Fig. 1) and low index Ni surfaces.

| | (100) fcc | (111) hcp | (111) fcc |
|---|---|---|---|
| $Ni_{38}$ + C | 8.32 | 7.35 | 7.20 |
| Ni surface + C | 8.49 | 7.31 | 7.24 |
| Coordination number | 4 | 3 | 3 |

RESEARCH ARTICLE

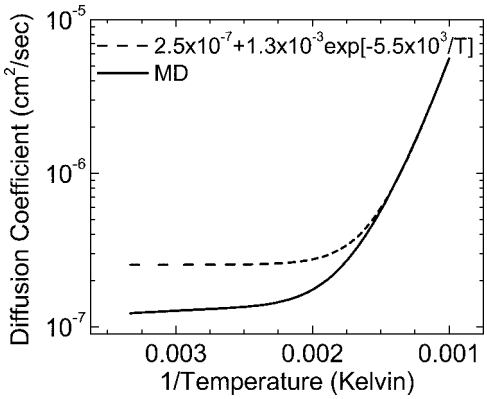


**Fig. 2.** Diffusion coefficient as a function of temperature. See discussion in text.

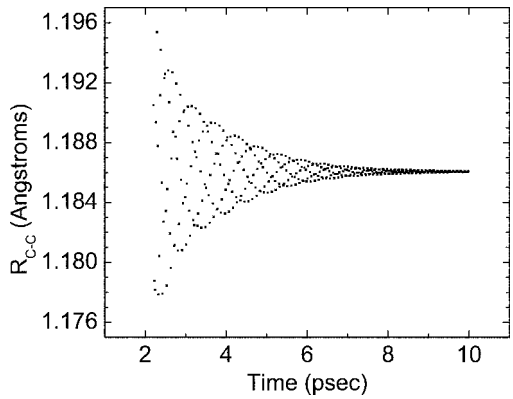


**Fig. 3.** Plot of samplings of the C–C distance as a function of time showing the formation of a carbon dimer in the semiempirical MD simulation of $Ni_{38}C_2$ cluster.

atures. At lower temperatures, the available energy was not sufficient to overcome the small activation barrier, 0.48eV, and the C atoms basically vibrate in local energy minima.

Semiempirical MD calculations were also used to examine the diffusion process of C in small Ni clusters. In this study, semiempirical quantum mechanics[31–34] was used (AM1[31] for C–C interactions and ZINDO[34] for Ni atoms) to compute the instantaneous potential of the Ni cluster and C atoms for each MD integration time step. Although semiempirical methods require less computer resources than *ab initio* methods, they are still computationally intensive. As such, only small nickel clusters ($Ni_{38}$) were studied using this technique. In these simulations we examined the molecular mechanism for diffusion of multiple C atoms within a given Ni cluster.

One interesting but not terribly surprising observation was that as the amount of carbon increased, the diffusion coefficient decreased independent of temperature. Examination of the dynamics associated with this phenomenon revealed that the C atoms tend to diffuse to other C atoms within the Ni cluster and form carbon dimers and trimers. Further examination showed that these multi-carbon atom clusters were actually chemically bonded, having the typical vibrational frequency of a C–C (diatomic) or C–C–C (triatomic) molecular fragment (as determined from the semiempirical quantum simulations). As evidence of clustering, we show in Figure 3 a plot of the C–C distance as a function of time. The convergence of this distance to the carbon dimer bond length is consistent with bond formation). The formation of these small carbon fragments might indicate the initial process involved in the overall growth of CNTs catalyzed by transition metals.

## 4. CARBON-METAL "FLAKE" CALCULATIONS

In this section, a number of energies needed in the calculations to be described below are calculated from first principles. We begin by considering small, flattened "flakes" that may be viewed as having been cut from an unrolled nanotube. The flakes are two-dimensional, and none of the strain energy due to rolling-induced curvature has been included in the calculations. Initially, we followed Lee et al.,[8b] and chose a flake consisting of five carbon hexagons, as shown in Figure 4a. After establishing that our results agreed well with those of Ref. 8b, in which similar computational approaches were used, the flake size was cut down to the three hexagons (14 C atoms) shown in Figure 4b so that a large number of calculations could be carried out on an accelerated basis. The agreement between results for the five and three hexagon calculations was

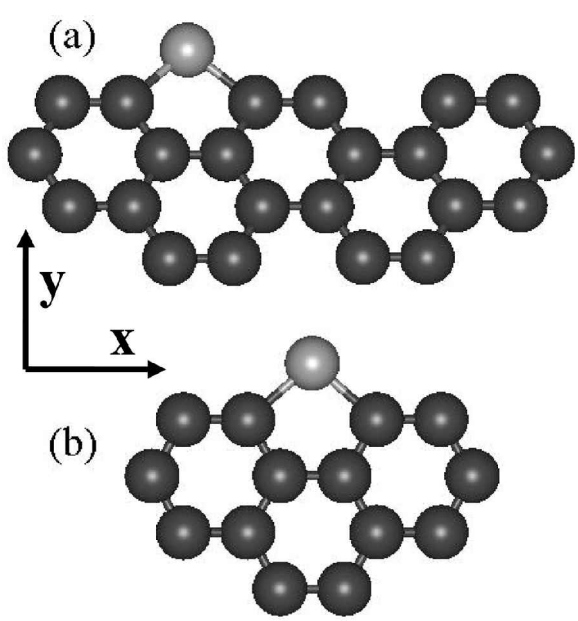


**Fig. 4.** Flakes used in calculation of binding of metal atoms at pentagon sites. (a) Five-hexagon flake used in initial calculations. (b) Three-hexagon flake used in most of the subsequent calculations. Dark spheres represent C atoms. Light spheres represent a metal atom.

excellent. The main reason for this agreement is probably that the C bonds, as in many organic systems, are quite well localized and therefore additive to a good approximation.

The initial set of calculations consisted of adding C, Cu, Au, Ni, Fe, and Co at the indicated site on Figure 4b to form a pentagon. The main purpose of these calculations was to determine whether there are any clear differences between metals that are good catalysts and those that are not. From a more general perspective, the formation of pentagons in the hexagonal graphitic network has been shown to be a key element in the nucleation of carbon nanotubes, "onions," and cones.[9]

The numerical techniques used the local spin density approximation and Gaussian orbitals as implemented in the NWChem software collection.[27] The simple Slater exchange functional was used and the Gaussian-type orbitals for the carbon atoms came from the standard 6-311G basis set. An effective-core potential approach used the CRENBL basis set with the following number of electrons treated by the effective potential: Cu(10), Au(60), Ni(10), Co(10), and Fe(10). The NWChem suite of programs is freely available and the part we utilized is quite similar to the commercially available software used in Ref. 8b.

Table II shows the results of the binding energy calculations for the metals indicated. Because the flake is envisioned as having been cut from a SWNT, no effort was made to carry out a general energy minimization with respect to all atomic displacements. Instead, the flake was assumed to be flat, and energy minimization was carried out only with respect to displacement of the metal atoms in the *y* direction. With the following definitions,

$E(A)$ — energy of isolated $A$ atom,
$E(C_N)$ — energy of a planar "flake" with $N$ carbon atoms,
$E(C_N, A)$ — energy of $C_N$ flake plus 1 $A$ atom,

the binding energy of an $A$ atom to an $N$ atom carbon flake is given by

$$E_b(A, N) = -\{E(C_N, A) - [E(C_N) + E(A)]\} \quad (4)$$

The sign convention has been chosen to make $E_b$ positive.

It can be seen from Table II that the binding energies of the Cu and Au atoms into the pentagon are about 1 eV less than those of the other metal atoms, which are about ½ eV less than that of a C atom (also in the pentagon position). These differences are too large and consistent with each other to be the result of the computational approximations that were made. Consequently, we view them as a reliable guide to the relative interaction energies of the metal atoms with the carbon flakes.

**Table II.** Binding energies (in eV) of metal atoms in a pentagon position to the three-hexagon flake of Figure 4b.

| Atom A | $E_b$ (A, 14) |
|---|---|
| C | 6.33 |
| Fe | 5.86 |
| Co | 5.94 |
| Ni | 5.87 |
| Cu | 5.05 |
| Au | 4.84 |

## 5. CLASSICAL NUCLEATION THEORY FOR NANOTUBES, AND THE CONNECTION WITH FIRST PRINCIPLES CALCULATIONS

### 5.1. Background

It has been demonstrated by Tománek and co-workers[35] that the use of concepts and approximations from classical elasticity theory is surprisingly fruitful even in work on nanostructured materials such as CNTs. In a recent paper by Kuznetsov and co-workers,[6] classical nucleation theory, elasticity approximations, and thermodynamical analysis were used to study the formation of critical nuclei for CNT formation. To set the stage for this section and introduce the ideas we are interested in here, certain aspects of their work are briefly summarized. We then show how first-principles calculations of the type discussed above can be used to estimate some of the relevant quantities entering the continuum calculations. This is the objective of the discussion, and no attempt will be made to calculate the critical radius, or nucleation rate, at this time.

In Ref. 6, the change in the Gibbs free energy, $\Delta G$, for the formation of a thin carbon nucleus is expressed as a sum of several terms. For a circular nucleus of radius $r$ and height $h$, it is convenient to make the $r$-dependence of $\Delta G$ explicit by writing

$$\Delta G = r^2 h \Delta G_{\text{bulk}} + r\Delta G_{\text{edge}} + r\Delta G_{\text{st}} + r^2 \Delta G_{\text{ad}} \quad (5)$$

The first three terms are relatively straightforward and have the following definitions:

$\Delta G_{\text{bulk}}$ is related (within a constant) to the change in free energy when 1 mole of C precipitates out from the metal-carbon solution. For a SWNT, it is not clear how it should be treated, but it would appear to be related to the reordering of the in-plane bonding not associated with any edge or surface effects.

$\Delta G_{\text{edge}}$ is the energy that arises when the dangling bonds at the edge of the flake are filled by interaction with the metal catalytic particle. This requires that the flake be bent, which introduces strain.

$\Delta G_{\text{st}}$ is the energy introduced by the above strain.

$\Delta G_{\text{ad}}$ is closely related to the adhesion of the carbon embryo to the catalytic metal particle from which it is being lifted, but the interaction of the top surface of the flake with the ambient gas is also to be included.

These terms in slightly different form are discussed in some detail in Ref. 6, in which an expression for the critical radius of the nucleus is found in the usual way by minimizing $\Delta G$ with respect to the radius. This gives

$$r_{\text{crit}} \nabla (\Delta G_{\text{edge}} + \Delta G_{\text{st}})/2\,(h\Delta G_{\text{bulk}} + \Delta G_{\text{ad}}) \qquad (6)$$

It can be seen that whether or not it is possible for nucleation to occur depends on the relative magnitudes of $\Delta G_{\text{edge}}$ and $\Delta G_{\text{st}}$. If the energy gained by satisfying the dangling bonds on the edge of the small nucleus is greater than the energy increase associated with the introduction of the bending strain, nucleation may occur; otherwise it definitely will not. These are the only two terms we will be concerned with here, and no attempt is made to calculate the critical radius itself for this article; we hope to do so at a later date.

### 5.2. Calculation of Strain Energy Due to Pentagon Formation

We first consider the strain energy $\Delta G_{\text{st}}$ introduced by the closure of a SWNT of ~0.7 nm radius by a $C_{30}$ cap; $\Delta G_{\text{edge}}$ will be considered in the next subsection.

The total binding energies of the 60 C atoms in the $C_{60}$ buckyball and of the 30 C atoms in one-half of an undistorted buckyball, shown in Figure 5, were first calculated. These are given by

$$E_{\text{b}}(\text{bb}) = -\{E_{\text{tot}}(\text{bb}) - 60{*}E\,(\text{C})\} \qquad (7)$$

and

$$E_{\text{b}}(\text{bb}/2) = -\{E_{\text{tot}}(\text{bb}/2) - 30{*}E\,(\text{C})\} \qquad (8)$$

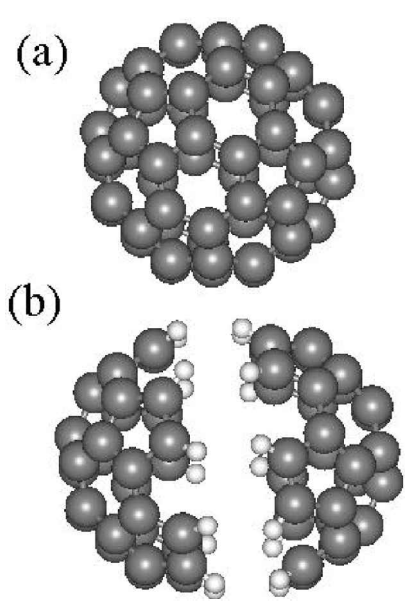


**Fig. 5.** Illustration of how the dangling bonds energy was calculated. Two halves of a buckyball are bound together by the energy gained when the dangling bonds are eliminated.

where, as before, $E$ (C) is the total energy of an isolated C atom.

Because of the mixture of pentagons and hexagons in the $C_{60}$ molecule, the environment of each carbon atom is not quite the same, even though the 3-fold coordination holds at each site. The average binding energy per C atom in the $C_{60}$ molecule was found to be 8.26 eV/atom. There are no dangling bonds in this structure.

By contrast, $E_{\text{b}}$(bb/2) of the unrelaxed hemispherical cap was found to be only 7.16 eV/atom, almost 1 eV less than that of $C_{60}$. There are 6 pentagons, 5 completed hexagons, and 10 dangling bonds in the cap. The dangling bonds introduce a large energy not directly related to the strain and this must be subtracted out for all those structures having such bonds. This was done in the following way.

The binding energy of the two halves of a buckyball to one another comes from the elimination of the 10 dangling bonds. To find it, the difference in energies between the complete $C_{60}$ and the sum of its two separated halves is calculated; that is,

$$\Delta E = -\{E_{\text{b}}(\text{bb}) - 2E_{\text{b}}(\text{bb}/2)\} = -\{E_{\text{tot}}\,(\text{bb}) - 2{*}E_{\text{tot}}\,(\text{bb}/2)\} \qquad (9)$$

$\Delta E$ was found to be 6.59 eV/bond. This is a key number for subtracting out the effects of the dangling bonds and arriving at the pure strain energy in our simplified approach.

In the next step, the binding energy, $E_{\text{b}}(C_{30})$, of a flat, almost circular flake containing 30 C atoms was calculated. There were 14 dangling bonds in the structure we used, but no strain. $E_{\text{b}}(C_{30})$ was found to be 7.20 eV/atom. Despite the larger number of dangling bonds, the average energy per bond is just slightly greater than it is in a half buckyball. This reflects the influence of strain in the latter, curved structure.

Finally, the contributions of the dangling bonds to the curved and flat structures can be subtracted out from $E_{\text{b}}$(bb/2) and $E_{\text{b}}(C_{30})$ and the strain energy, $E_{\text{st}}$, defined as the difference between the remaining energies, can be computed. This gave for $E_{\text{st}}$ a value of 25.2 eV. The circumference of the cap is 2.2 nm so the strain energy/unit length from this calculation is 11.4 eV/nm.

In Ref. 6, the strain energy was estimated from elasticity theory to be given by $Q_c\lambda/4.5h$, with $\lambda$ being the edge length, $Q_c = 4.4$ eV, and $h = 0.34$ nm, the interlayer spacing in graphite, which is very nearly the radius of $C_{60}$. With $\lambda = 2.2$ nm, this expression gives 6.3 eV/nm for $E_{\text{st}}$. However, the value obtained in Ref. 35 of $E_{\text{st}}$ ~22 eV is much closer to our result.

### 5.3. Estimates of Edge Free Energy

The simplest estimate for the edge free energy of the hemispherical $C_{30}$ cap just puts the edge atoms in the pentagon position of Figure 4b and uses the indicated binding energies from Table II. Because there are 10 dangling bonds, an

edge energy for Ni, for example, of 58.7 eV is found. After dividing by the circumference, the specific edge energy of 26.7 eV/nm is obtained (and essentially is the same value for Fe and Co). This is likely to be an overestimate for two reasons. First, it provides an almost ideal bonding, from the standpoint of cap formation, of the Ni atom to the C flake and ignores all geometrical considerations associated with fitting the circular nanotube onto the planar catalytic particle. Secondly, an examination of a buckyball model quickly shows that to complete the dangling bonds simply by adding Ni atoms at pentagon sites would seem to put some of the Ni atoms too close together. Nevertheless, the estimates of the edge free energies from Ref. 6, using thermodynamic data for Fe, Ni, and C give 18.6 eV/nm for Ni and 23.8 eV/nm for Fe, quite close to our calculated values. For Cu and Au we obtain, respectively, 23 and 22 eV.

### 5.4. Critical Radius

Calculation of $\Delta G_{edge} + \Delta G_{st}$ from Eq. 6 for the critical radius gives ~1.5 eV/nm for Fe, Co, and Ni and ~−2.5 eV/nm for Cu and Au. The negative value means that a stable nucleus will not form for Cu and Au. Although these results are exactly what is needed to explain the occurrence, or lack thereof, of nucleation for these elements, the calculations are still too simplified and approximate at this point to be definitive. As stated above, we hope to pursue this matter further at a later date.

We conclude that there is very encouraging agreement between the results based on the atomistic first-principles and the continuum elasticity/thermodynamics mesoscopic calculations. More importantly, the results may be pointing the way to an understanding of the CNT catalytic mechanism. Also, although there are no dynamics explicitly involved in the calculations, they do represent an elementary type of multiscaling that may be implemented in more detail as needed.

## 6. FUNDAMENTAL CATALYTIC MECHANISM

Ideally, we would like to argue that there is a fundamental catalytic mechanism that operates regardless of the method for forming the SWNTs and then, of course, to be able to identify it. Although this goal is still elusive, some of our results may represent progress in reaching it. In this connection, and as discussed below, our results are consistent with aspects of the mechanism proposed by Smalley, Tománek, and co-workers in Ref. 8. In this scenario, the primary role of the catalyst is to prevent the formation of pentagons of C, which, as seen above, would introduce curvature, cause the nanotube to become capped, and cause growth to cease. This model assumed that the concentration of Ni was small compared with that of C and that a single Ni atom could organize the growth of the nanotube by "scooting" around the circumference of the tube. Consequently, it is sometimes referred to as the scooter model. In our approach, the nanotube is always growing out of a relatively large catalytic particle, and there is no need to invoke the scooting action.

### 6.1. Binding of Pentagons to Hexagons

In this subsection, the binding energies of carbon and metal atoms in a hexagon configuration are compared with their energies in two separated pentagon sites, as illustrated in Figure 6. To calculate the hexagon energies, $E_h$, a C atom was put at a normal hexagon site in a 16-atom flake. A metal atom was placed at the other hexagon site (lighter circle in Fig. 6b). Exploratory calculations were carried out by first moving the metal atom in the $x$ direction and then in the $y$ direction. The sensitivity of the binding energy to displacements of the metal atoms in the $x$ direction was not great and the C–M $x$ separation was subsequently fixed at 0.9 A rather than the C–C equilibrium distance of 0.71 A (which is still a substantial increase in this separation). The metal atoms were then displaced in the $y$-direction and the minimum energy with respect to this displacement was found. This generated the curves of $E_h(x)$ shown in the various panels of Figure 7. The curve for Co overlaps almost completely that for Ni and is not given.

The panels also show, as a horizontal line, the energies, $E_p$, of two well-separated pentagons (one with C and one with a metal), as given by

$$E_p = E_b(\mathrm{C}) + E_b(\mathrm{M}) \tag{10}$$

with $E_b$ (C) and $E_b$ (M) taken directly from Table II. It can be seen that for all the metals except Cu and Au, the $E_h$ curves drop below the $E_p$ lines, signifying that in these

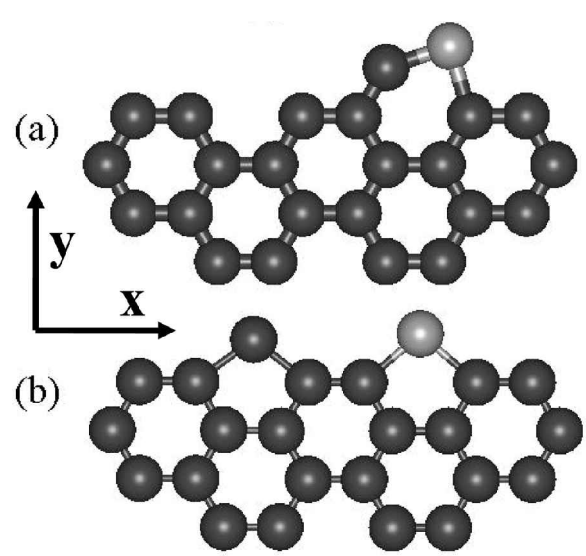


**Fig. 6.** Two well-separated pentagons, one with a C atom and one with a metal atom, may combine to form a distorted hexagon if the total energy can be lowered in that way.

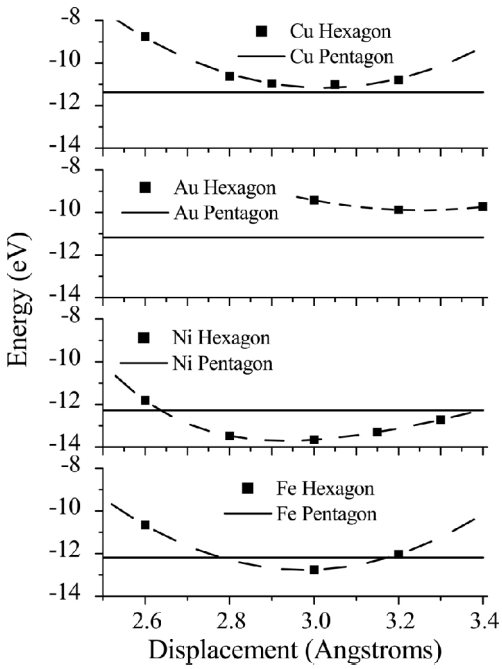


**Fig. 7.** Hexagon energy as a function of the position of the metal atom. Details are given in the text. The straight line is the energy of two separated pentagons. The results are virtually identical for Co and Ni. The hexagon configuration is preferred for Ni, Fe, and Co, but not for Au and Cu.

cases it is energetically favorable to have the metal in the hexagon configuration. These results are summarized in Table III in which the energy differences $\Delta E = E_h - E_p$ are also given. $\Delta E > 0$ means that the C–M hexagon is stable against breakup into the two pentagons.

The results obtained above for Ni are quite consistent with those reported by Tománek and co-workers in Ref. 8 for their five hexagon flakes. Here, however, this type of calculation has been extended to several other metals, and the results are consistent with our ideas about the catalytic activity of the various metals.

Although the results to this point are encouraging, what is needed now is to show the actual functioning of the catalytic atoms by carrying out MD simulations along the lines indicated in Section 3 for the diffusion coefficient. To do this will require going well beyond what has been described here.

**Table III.** Comparison of binding energies of a carbon and a metal atom in a hexagon to the binding energies in separated pentagons. $\Delta E > 0$ means the C–M hexagon is stable against breakup into separated pentagons.

| | $E_h$ (eV) | $E_p$ | $\Delta E$ |
|---|---|---|---|
| C | −15.75 | −12.66 | +3.09 |
| Cu | −10.96 | −11.38 | −0.42 |
| AU | −9.88 | −11.17 | −1.29 |
| Ni | −13.66 | −12.29 | −+1.37 |
| Co | −13.64 | −12.27 | +1.37 |
| Fe | −12.76 | −12.19 | +0.57 |

## 7. SUMMARY, CONCLUDING REMARKS, AND FUTURE DIRECTIONS

The binding of a C adatom on various Ni surfaces and Ni cluster facets was calculated using DFT, and the magnitude and ordering of adsorption energies for the sites for C atom adsorption on both $Ni_{38}$ cluster and the extended Ni surfaces are essentially the same. Both $Ni_{38}$ cluster and low-index Ni surface results show that the (100) site is favored. These computational results are qualitatively consistent with experimental results for binding of C to Ni clusters and low-index Ni surfaces. A preliminary explanation may be found in the local bonding character of carbon,[24, 26] and the well-defined facets on $Ni_{38}$. We expect that this preference sequence and the adsorption energy at the most stable site should also be maintained for larger Ni clusters. Even though this information is only available via theory, it does not directly answer questions such as why clusters, rather than extended surfaces, are effective catalysts for SWNT growth. To address this in future work, we will compute adsorption and diffusion energetics of C on smaller $Ni_n$ and $Fe_n$ clusters for $n \sim 2$ to 10, where it is known that the bonding energy varies strongly with cluster size.[25, 26] There is some evidence supporting the idea that these small clusters provide important catalytic activity in the HiPco process.[36] However, contrasting points of view exist in which the important catalytic activity in the HiPco process occurs for metal clusters of diameter near 1 nm.[37]

MD calculations were used to study bulk diffusion of C in Ni clusters as a function of C concentration and temperature. The diffusion coefficient shows the expected exponential increase with temperature at high temperatures. It decreases as the C concentration increases due to clustering of the C atoms within the Ni. Electronic structure calculations of the binding energy of various metal atoms to a 14-atom C flake show that Au and Cu are less tightly bound than Ni, Co, and Fe by about 1 eV. Calculations on $C_{60}$, $C_{30}$, and a 30-atom planar array allow the strain energy due to cap formation to be determined. The edge energy that arises from the completion of dangling bonds is then calculated. These quantities are compared with values obtained from a determination of the classical nucleation theory of CNT growth. Finally, comparison of the binding of a carbon and a metal atom in a hexagon to that in separated pentagons indicates that for the catalytic metals the hexagon is stable against the breakup into two pentagons. This may provide a mechanism for preventing nanotube closure due to stable pentagon formation, as has been suggested in Ref. 8.

The future directions of this research are expected to evolve along the following lines. In the surface related work, the surface diffusion coefficient of C on Ni as a function of temperature will be calculated. Following the strategy already used in the flake calculations, differences between the computed results for the good (Ni, Fe, and Co)

and the bad (Au and Cu) catalysts will be sought and correlated with their catalytic activities. Particular emphasis will be put on small (~5 atom) clusters.

The work on bulk diffusion will continue to investigate the construction of suitable Ni–C interaction potentials for MD calculations. The interaction of C atoms to form clusters in the bulk and at the surface of the Ni particles will be studied. The formation of ring segments at or near the surface will be of particular interest.

It should be fairly straightforward to extend the calculations to do a more complete job of relating the elasticity and thermodynamic parameters to first-principles calculations. This will involve calculating $\Delta G_{\text{bulk}}$ and $\Delta G_{\text{ad}}$ in Eq. 6. However, we must first determine exactly what $\Delta G_{\text{bulk}}$ corresponds to because it is clearly not just the bulk binding energy of a C atom in a hexagon. Most likely it is the energy released when an amorphous-like C layer reorders to form a hexagonally bonded film.

For the basic catalytic mechanism discussed in Section 5, a reliable molecular dynamics simulation will eventually be required. A first step in this direction will be to use the interaction potentials already obtained in the bulk calculations of Section 3. The focus will be on trying to identify a rate-determining step that can be compared with a modified scooter-type mechanism.

**Acknowledgment:** This work was supported by the Laboratory Directed Research and Development (LDRD) program at Oak Ridge National Laboratory (ORNL), managed by UT-Battelle for the U.S. Department of Energy under Contract DE-AC05-00OR22725. Accordingly, the U.S. Government retains a nonexclusive, royalty-free license to publish or reproduce the published form of this contribution or allow others to do so for U.S. Government purposes.

## References and Notes


1. (a) R. T. K. Baker and P. A. Harris, *Chemistry and Physics of Carbon*, edited by P. L. Walker and P. A. Thrower, Marcel Dekker, New York (1978), Vol. 14, p. 83; (b) R. T. K. Baker, *Carbon* 27, 315 **(1989)**.
2. Alstrup, *J. Catal.* 109, 241 **(1988)**.
3. (a) E. C. Bianchini and C. R. F. Lund, *J. Catal.* 117, 455 **(1989)**; (b) S. A. Safvi, E. C. Bianchini, and C. R. F. Lund, *Carbon* 29, 1245 **(1991)**.
4. P. Chitrapu, C. R. F. Lund, and J. A. Tsamopoulos, *Carbon*, 30, 285 **(1992)**.
5. H. Kanzow and A. Ding, *Phys. Rev. B* 60, 11180 **(1999)**.
6. V. L. Kuznetsov, et al., *Phys. Rev. B* 64, 235401 **(2001)**.
7. A. Maiti, C. J. Brabec, C. Roland, and J. Bernholc, *Phys. Rev. B* 52, 14 850 **(1995)**.
8. (a) A. Thess et al., *Science* 273, 483 **(1996)**; (b) Y. H. Lee, S. G. Kim, and D. Tománek, *Phys, Rev. Lett.* 78, 2393 **(1997)**.
9. (a) A. Krishnan, et al., *Nature* 388, 451 **(1997)**; (b) R. E. Smalley and B. I. Yakobson, *Solid State Commun.* 107, 597 **(1998)**.
10. (a) J. Gavillet, et al., *Phys. Rev. Lett.* 87, 275504 **(2001)**; (b) J. Gavillet, et al., *Carbon* 40, 1649 **(2002)**.
11. X. Fan, et al., *Phys. Rev. Lett.* 90, 145501 **(2003)**.
12. D. Vanderbilt, *Phys. Rev. B* 41, 7892 **(1990)**.
13. G. Kresse and J. Furthmüller, *Comput. Mater. Sci.* 6, 15 **(1996)**.
14. Computational methods based on linear combination of atomic orbitals using Gaussian-type orbitals, similar to those used in Section 4, were also applied to the $Ni_{38}$ cluster. Results for $Ni_{38}$ are not presented here because of difficulties in numerical convergence. By comparison, the convergence properties of the planewave, pseudopotential approach are better.
15. J. P. Perdew, et al., *Phys. Rev. B* 46, 6671 **(1992)**.
16. M. C. Vargas, et al., *J. Phys. Chem. B* **105**, 9509 **(2001)**, and references therein.
17. For further details, see Q. Zhang, J. C. Wells, X. G. Gong, and Z. Zhang, *Phys. Rev. B,* to be published.
18. (a) J. Ho, et al., *J. Chem. Phys.* 99, 8542 **(1993)**; (b) A. A. Radzig and B. M. Smirnov, *Reference Data on Atoms, Molecules, and Ions,* Springer-Verlag, Berlin, 1985. *Note:* For both Ni and C, the atomic reference energy used is a triplet state, with triplet-singlet energy difference taken as 1.2 eV for C and 0.4 eV for Ni.
19. G. S. Painter and F. W. Averill, *Phys. Rev. B* 26, 1781 **(1982)**.
20. F. W. Kutzler and G. S. Painter, *Phys. Rev. B* 45, 3236 **(1992)**.
21. C. Rey, et al., *Phys. Rev. B* **62**, 12640 (2000) and references therein.
22. J. Zhu, X. W. Wang, and S. G. Louie, *Phys. Rev. B* 45, 8887 **(1992)**.
23. For summary, see D. J. Klinke II, et al., *J. Catal.* 178, 540 **(1998)**.
24. L. C. Isett and J. M. Blakely, *Surf. Sci.* 58, 397 **(1976)**.
25. F. Liu and P. B. Armentrout, private communication.
26. R. Liyanage, X.-G. Zhang, and P. B. Armentrout, *J. Chem. Phys.* 115, 9747 **(2001)**.
27. D. E. Bernholdt, et al., *Int. J. Quant. Chem.* 29, 475 **(1995)**; www.emsl.pnl.gov:2080/docs/nwchem/nwchem.html.
28. (a) H. Basch, et al., *J. Chem. Phys.* 73, 4492 **(1980)**; (b) E. M. Nour, et al., *J. Chem. Phys.* 86, 4779 **(1987)**; (c) K. P. Huber and G. Herzberg, *Constants of Diatomic Molecules,* Van Nostrand Reinhold, New York, 1979.
29. S. Mayo, et al., *J. Chem. Phys.* 94, 8897 **(1990)**.
30. Y. J. Lee, et al., *Comp. Phys. Comm.* 142, 201 **(2001)**.
31. J. Sadlej, *Semi-Empirical Methods of Quantum Chemistry*, Ellis Harwood, Chichester, UK, 1985.
32. J. J. P. Steward, *Encyl. Comput. Chem.* 3, 2000 **(1998)**; J. J. P. Steward, *Encyl. Comput. Chem.* 2, 1513 **(1998)**.
33. A. J. Holder, *Encyl. Comput. Chem.* 1, 8 **(1998)**.
34. M. C. Zerner, *Rev. Comput. Chem.* 2, 313 **(1991)**.
35. D. Tománek, et al., *Phys. Rev. B* 48, 15 461 **(1993)**. This paper has several other references to the work relating elasticity and first-principles calculations in CNTs.
36. M. J. Bronikowski, et al., *J. Vac. Sci. Technol. A* 19, 1800 **(2001)**.
37. I. W. Chiang, et al., *J. Phys. Chem. B* 105, 8297 **(2001)**.


Received: 7 May 2003. Revised/Accepted: 1 August 2003.